NASA TM X- 70442

NEAR EARTH MAGNETIC DISTURBANCE IN TOTAL FIELD AT HIGH LATITUDES

I. SUMMARY OF DATA FROM OGO'S 2, 4, AND 6

R. A. LANGEL

AUGUST 1973

GSFC ———— GODDARD SPACE FLIGHT CENTER ————
GREENBELT, MARYLAND

NEAR EARTH MAGNETIC DISTURBANCE IN

TOTAL FIELD AT HIGH LATITUDES

I. SUMMARY OF DATA FROM OGO'S 2, 4, AND 6

by

R. A. Langel

Laboratory for Space Physics

Goddard Space Flight Center

Greenbelt, Maryland 20771

August 1973

NEAR EARTH MAGNETIC DISTURBANCE IN

TOTAL FIELD AT HIGH LATITUDES

I. SUMMARY OF DATA FROM OGO'S 2, 4, AND 6

by

R. A. Langel

ABSTRACT

Variations in the total (i.e. scalar) magnetic field data from the polar orbiting OGO-2, 4, and 6 spacecraft (altitudes 400-1510 km) are summarized for invariant latitudes above 55°. Data from all degrees of magnetic disturbance are included. The data are presented in terms of the quantity ΔB (= measured field magnitude minus the field magnitude from a spherical harmonic model of the quiet field). The total field variations at the satellite form two regions: (1) a region of positive ΔB between about 22^h and 10^h MLT (magnetic local time), with its maximum near 3^h and 72°, and (2) a region of negative ΔB between about 10^h and 22^h MLT with its maximum near 15^h and 75°. In the negative ΔB region, $|\Delta B|$ is greatest in summer and least in winter and shows a substantial decrease with increasing altitude. $|\Delta B|$ in the positive ΔB region, on the other hand, shows no seasonal variation and only a small decrease with increasing altitude. $|\Delta B|$ increases with the Ap index in both regions.

CONTENTS

TABLES

PRECEDING PAGE BLANK NOT FILMED

ILLUSTRATIONS

NEAR EARTH MAGNETIC DISTURBANCE IN

TOTAL FIELD AT HIGH LATITUDES

I. SUMMARY OF DATA FROM OGO'S 2, 4, AND 6

A complete survey of the near earth magnetic field magnitude was carried out by the Polar Orbiting Geophysical Observatories (OGO 2, 4, and 6) also known as the "POGO" satellites. This paper presents a survey of the average properties of variations in total magnetic field strength at invariant latitudes greater than 55°. Extensive interpretation of the data to be presented is not included in the present paper, but is planned for several companion papers.

Some characteristics of the POGO orbits are as follows:

Satellite	Launch Date	Inclination	Perigee (km)	Apogee (km)
OGO 2 (1965 81A)	Oct. 14, 1965	87.3°	410	1510
OGO 4 (1967 73A)	July 28, 1967	86.0°	410	910
OGO 6 (1969 51A)	June 5, 1969	82.0°	400	1100

OGO 2 acquired data from launch until Oct. 2, 1967. Data were, however, limited to twilight local times (when the orbit was in full sunlight) because of an early failure in the attitude control system. OGO 4 operated almost continuously from launch until Jan. 19, 1969, and OGO 6 operated almost continuously until Aug. 29, 1970, and sporadically from then until June 1971. The present study includes OGO 6 data only up to December 1969, except for a small segment of data from March 1970.

The magnetic field, $\vec{B}$, is the vector sum of magnetic fields from several sources. We write $\vec{B} = \vec{M} + \vec{Q} + \vec{D}$, where $\vec{M}$ is the main field of the earth, including crustal anomalies and long term (or secular) changes, $\vec{Q}$ is the variation in $\vec{B}$ present on all days (the quiet daily variation), and $\vec{D}$ is the additional variation present on magnetically disturbed days. OGO's 2, 4, and 6 measured the magnitude, but not the direction, of $\vec{B}$, so that the quantity analyzed is $\Delta B = |\vec{B}| - |\vec{M}|$.

INSTRUMENTATION AND DATA ACCURACY

The measurements were taken with optically pumped, self-oscillating rubidium vapor magnetometers (Farthing and Folz, 1967). These instruments measured the absolute scalar field to better than 2γ ($10^9\gamma = 1$ tesla), as determined by direct comparison with proton precession magnetometers before flight. Digitization was performed onboard the spacecraft using a sampling interval of 0.5 seconds for OGO's 2 and 4 and 0.288 seconds for OGO 6. Extraneous magnetic fields from the rest of the spacecraft were measured prior to launch and found to be below 1γ at the rubidium vapor sensor, which was mounted at the end of a 6 m. long boom.

Satellite characteristics and data accuracy are discussed in some detail by Langel (1967, 1973), Cain et al. (1967a), and by Cain and Langel (1971). The standard deviation of error estimates from all known sources of error, including inaccuracies in orbital position, was 5.63γ.

For the satellite data used in this study, $\vec{M}$ is approximated by a spherical harmonic model of the earth's main field, including secular change, derived using POGO data from especially selected quiet days. The method of derivation of such models is discussed by Cain et al. (1967b). Previous selections of data (Cain et al., 1967b; Cain and Langel, 1971) have utilized data from magnetically quiet times ($Kp \leqslant 1^-$). A scan of POGO data for $Kp \leqslant 1^-$ indicates, however, that there is occasionally some disturbance present even during periods of low Kp. In view of this we have also visually scanned the data plots and have eliminated any clearly disturbed passes. This procedure does not, of course, eliminate the $\vec{Q}$ field. In the fitting procedure, the data from all local times were used for each longitude, so that at a given longitude the daily average of $\vec{Q}$ will be included in $\vec{M}$. The daily variation of $\vec{Q}$ should still be discernible in $\triangle B$. Inasmuch as the data used in the fit span the entire interval under consideration in the subsequent analysis, the secular change of B should be well determined. It should be noted, however, that outside the period covered by the data (10/65 - 3/70), the secular change terms may not accurately represent the true field changes.

The fitting process used 51,223 points which were fit with the 120 coefficients given in Table 1 to a root mean square residual of 8γ.

Because the POGO data are of total field only and are taken in a limited altitude range, we are unable to separate sources of origin internal and external to the earth. Thus, any quiet time external field which varies slowly with altitude,

3

and is constant in MLT and longitude, will be regarded as part of $\vec{M}$ in the present study.

Models such as POGO(8/71) assume that field sources are absent from the region where measurements are made (400-1510 km) such that $\vec{B}$ is curl free and can be represented by a potential function. Because the conductivity normal to field lines at POGO altitudes is small, currents normal to field lines are believed to be negligible at all times; however, currents along magnetic field lines are likely at these altitudes. Several reasons exist for asserting that the POGO (8/71) model does not include an important contribution from field aligned currents. In particular, the geometry of disturbing fields from field aligned currents is such that the major effect is a change in direction of $\vec{B}$ rather than a change in magnitude. Since POGO data are measurements of field magnitude, not direction, and the POGO(8/71) model is determined from such data, the model should be unaffected by changes in field direction alone. If field aligned currents did cause a small variation in field strength, these variations are not likely to be constant in local time so that only an average would be included in the field model.

The geometrical argument also illuminates the physical meaning of the quantity ΔB at high latitudes, so it is profitable to illustrate the argument by the following computational results. At a particular location (R, θ, ϕ; geocentric), the ΔB which would be caused by a disturbing field of 1000γ is computed with the undisturbed field represented by a dipole. The disturbing field is taken to

4

be either purely in the R direction (geomagnetic -Z), purely in the θ direction (geomagnetic -X), or purely in the ϕ direction (geomagnetic Y). For the range of R considered (1-1.3 earth radii), the variation of ΔB with R is negligible, and by symmetry ΔB is independent of ϕ. ΔB versus latitude (= 90° - θ) is plotted in Figure 1 for disturbing fields in the R and θ directions; ΔB is negligible for disturbing fields in the ϕ direction. A disturbing field in the R direction causes a ΔB of nearly the same magnitude as the disturbing field, while a disturbing field in the θ direction is "less than 22% effective" in producing ΔB at and above auroral belt latitudes (65°). In view of these results, high latitude ΔB is interpreted as though it were ΔZ.

Field aligned currents will cause disturbing fields transverse to the undisturbed field which result in negligible ΔB, as in the computation for the ϕ direction discussed above.

That the POGO(8/71) model adequately represents $\vec{M}$ is perhaps best demonstrated by noting that truly quiet passes ($|\Delta B| \lesssim 10\gamma$, say) occur frequently in the data at times when observatory data is also classed as quiet.

The standard deviation of the data used to generate the POGO(8/71) model with respect to that model is only 8γ, which is not much greater than the 5.33γ estimated standard deviation of data errors. We conclude that the 8γ standard deviation of the data with respect to the model is a reasonable estimate of the degree to which the model approximates $\vec{M}$ for the altitude range and epoch of the observations.

SELECTION OF DATA FOR AVERAGING

MLT-invariant latitude patterns of ΔB are utilized to study the dependence of ΔB on season, magnetic activity level, and altitude. As simultaneous measurements from many satellites are not available, these studies utilize appropriate averages and the data are subdivided by the above mentioned parameters before averaging.

Division of the data by magnetic activity was based on the Kp indices; four ranges of Kp were chosen and characterized as to magnetic disturbance level as follows:

(1) Quiet, Kp = 0 to 0^+,

(2) Slightly disturbed, Kp = 1^- to 1^+,

(3) Disturbed, Kp = 2^- to 3^+ , and

(4) Very disturbed, Kp $\geqslant 4^-$.

The use of Kp rather than AE as a sorting index means that our results are not related to a particular phase of substorms. It will be shown that several main features of ΔB do not correlate well with AE. This fact, together with the unavailability of AE for 1969, and the lack of data from Soviet stations in AE for much of the time span of interest (as of this writing), led to the use of Kp as the best available index.

The term "season" is defined relative to the dipole coordinate system. For each data point we have computed the dipole latitude of the sub-solar point, θ_{sun}; the "geomagnetic seasons" are then defined in terms of θ_{sun}, namely:

6

$|\theta_{sun}| < 10°$ is equinox,

$\theta_{sun} > 10°$ is northern summer, and

$\theta_{sun} < -10°$ is northern winter.

Thus, conditions exist such that a data point from a particular geographic season will fall in a different geomagnetic season.

Data from the following altitude ranges were considered together: < 550 km., $550-700$ km., $700-900$ km., and >900 km. The polar regions of each hemisphere were partitioned into 421 segments of approximately equal area. One data point was selected from each satellite pass for each segment traversed by that pass. All of the selected data within each segment for a particular Kp range, season, and altitude range were averaged and the results were plotted and contoured in a magnetic local time-invariant latitude coordinate system.

Table 2 gives the average altitude, the average number of points, and the average magnetic disturbance level (Ap index) for each plot (or data division). The range of average Ap $(\overline{Ap})$, for altitude and seasonal data divisions within a given Kp range, is small for the three lowest Kp ranges, so that comparisons between data divisions are not biased by the data selection. For data divisions where Kp $\geqslant 4^-$, $\overline{Ap}$ ranges between 30 and 48, which is a large enough difference so that some caution in comparisons between data divisions is advised.

From Table 2 it is apparent that the number of points over which averages are taken varies considerably between data divisions. Because more points are

available for Kp = 2⁻ to 3⁺ than for the other Kp ranges, the statistics are most favorable for this range and it will be utilized for most of our examples. In general, adequate numbers of points are also available for the range Kp = 1⁻ to 1⁺, but for Kp = 0 to 0⁺ and Kp ⩾ 4⁻ some divisions occur in which $\overline{N}$ is small so that the results must be interpreted with some care.

Data errors due to inaccurate orbit information or to strictly data reduction/telemetry problems are unlikely to be systematic in MLT and invariant latitude. Such errors will, therefore, tend to be averaged out and so should not affect these results.

GENERAL FEATURES OF AVERAGE ΔB PATTERNS, DEFINITION OF POSITIVE AND NEGATIVE ΔB REGIONS

Four representative contour plots have been selected and are given in Figure 2. The basic disturbance pattern of ΔB, for all seasons and Kp levels, is positive from near 22ʰ to near 10ʰ MLT and is negative from near 10ʰ to near 22ʰ MLT. These regions are designated the positive ΔB region and the negative ΔB region, respectively. Both regions have broad maxima. In the positive ΔB region the maximum is between 2ʰ and 5ʰ MLT, and in the negative ΔB region it is between 14ʰ and 18ʰ MLT. Equatorward of approximately 65°, ΔB reverses, but the peak value in the reversed region is less than one fifth the magnitude of the peak value in the poleward region.

Because of the large number of averages computed (421 per data division), it is impractical to present all of the relevant statistical information. In general,

the standard deviation (σ) of each average is less than the maximum $|\Delta B|$ nearest to that average, i.e., $\sigma \leqslant |\Delta B|_{max}$. These rather large values of σ reflect the great variability of ΔB magnitudes from pass to pass. Examination of individual passes, however, makes it clear that the regions of positive and negative ΔB are always located in MLT and latitude as described above, although the boundaries between the regions ($\sim 10^h$ and $\sim 22^h$ MLT) may vary by about $\pm 3^h$ from their average location.

A "typical" individual pass from OGO 4 is shown in Figure 3. The thin line indicates the satellite path and serves as the "baseline" for ΔB. The scale for ΔB is given by the short lines (scale lines) normal to the baseline; these project away from the baseline in the direction of positive ΔB, and a ΔB displacement normal to the baseline equal to the length of the scale line has a magnitude of 150γ. Labels on the scale line indicate the altitude and universal time when the satellite was at the position where the scale line meets the baseline. The positive and negative ΔB regions, each with peak disturbance magnitude near 110γ, are apparent in Figure 3 in the locations expected on the basis of the average data.

To make comparisons between data divisions (season, altitude, Kp), we define the "contour level of maximum disturbance" as the highest magnitude contour which encloses at least five contiguous (average) points. These contour levels are tabulated in Table 3.

From the standard deviation, the standard error, α, of each average is found by $\alpha = \sigma/\sqrt{n}$, where n is the number of points entering into the average.

Taking $\sigma \approx |\Delta B_{max}|$, an estimate of the standard error of the averages, $\alpha \approx |\Delta B_{max}|/\sqrt{n}$, is given in Table 4. $|\Delta B_{max}|$ is taken from the contour of maximum disturbance in the (positive or negative ΔB) region (Table 3), while n is estimated by $\overline{N}$ from Table 2.

While α may be a reasonable estimate of the standard error of an individual average, it is not obvious that the same error estimate applies to the contours. In general, the consistency of contiguous averages, particularly for $Kp = 1^-$ to 1^+ and $Kp = 2^-$ to 3^+, is such that one might assume that the contours approximate the true average ΔB to a greater accuracy than α. Because of the difficulty in assigning error estimates to the contours, error bars have been omitted from plots in the remaining sections of the chapter. Table 4 is meant to serve as a guide to estimating the errors in these figures.

ALTITUDE VARIATION

The variation of ΔB from the contour of maximum disturbance (Table 3) with altitude (from Table 2) is shown in Figures 4 and 5. Comparison of these plots indicates that $|\Delta B|$ decreases with altitude at a faster rate in the negative ΔB region than in the positive ΔB region. To be quantitative, where the data distribution permits a meaningful computation we have computed the percentage decrease of ΔB from altitudes <550 km. to altitudes >900 km. for each Kp and seasonal data division. The range of the percentage decrease is 0% to 64% over 19 data divisions in the positive ΔB region and 48% to 100% over 15 data divisions in the negative ΔB region. The average percentage decrease is 38% in the positive ΔB region and 87% in the negative ΔB region. Some

10

seasonal dependence is present in the percentage decrease, particularly in

the negative ΔB region where the percentage decrease is much greater in

winter (average = 98%) than in summer (average = 69%).

SEASONAL VARIATION

Comparison of northern and southern hemisphere data shows that the basic

ΔB pattern and contour levels are closely similar in both hemispheres for equiv-

alent season, altitude, and Kp range. The largest differences occur for Kp $\geqslant$

4^-, where the largest errors are present in the averages; we attribute no signi-

ficance to these differences. Because of the symmetry between hemispheres,

our discussion can be limited to the northern hemisphere with no lack of

generality.

Figures 4-5 serve to illustrate the seasonal variation of the two regions.

From Figure 4 it is apparent that, in the negative ΔB region, disturbance ampli-

tude is greatest in summer and least in winter for all Kp ranges (data for equinox

and winter for Kp = 0 to 0^+ were negligible at higher altitudes and so are not in-

cluded in the figure). The amplitude difference between seasons is quite large.

In contrast to the negative ΔB region, the positive ΔB region shows no sea-

sonal change within experimental error, as shown in Figure 5.

VARIATION WITH THE GLOBAL MAGNETIC DISTURBANCE INDEX Ap

$|\Delta B|$ is expected to increase with Ap, inasmuch as both quantities are

measurements of magnetic variation. Ap, however, is determined from mid-

latitude stations with a wide distribution in magnetic local time. It is of some

11

interest, therefore, to examine the dependence of ΔB on Ap in the positive and negative ΔB regions, which are limited in local time extent and confined to high latitudes. Figure 5 shows the variation of ΔB (from the contours of maximum disturbance in the northern hemisphere) with Ap for two altitude regions and all geomagnetic seasons.

The positive ΔB region again shows very little seasonal dependence, but a large seasonal dependence is apparent in the negative ΔB region, not only in the ΔB at each Ap, but also in the rate of increase of $|\Delta B|$ with Ap. In particular, the slope of the curve for summer is greatest and that for winter is least.

Both positive and negative ΔB regions show a tendency for the rate of increase of $|\Delta B|$ with Ap to decrease with increasing $|\Delta B|$. This is a weak tendency in the positive ΔB region but is a major feature in the negative ΔB region. Because this tendency is strong in the negative ΔB region, the overall rate of increase of $|\Delta B|$ with Ap is larger in the positive ΔB region than in the negative ΔB region.

SUMMARY AND CONCLUSIONS

Average ΔB patterns have been produced which indicate positive and negative ΔB regions between 22^h-10^h MLT and 10^h-22^h MLT, respectively. The data have the following characteristics:

(1) $|\Delta B|$ decreases with altitude in both the positive and negative ΔB regions. This decrease is small in the positive ΔB region and large in the negative ΔB region.

(2) The magnitude of ΔB exhibits no discernible variation with season in the positive ΔB region, whereas $|\Delta B|$ in the negative ΔB region is greatest in summer and least in winter.

(3) $|\Delta B|$ increases with increasing Ap (global disturbance index). This increase is more pronounced in the positive ΔB region than in the negative ΔB region.

Extensive interpretation of these data is presented in several companion papers. However, brief mention of the major results is appropriate. It is concluded that the negative ΔB region can be accounted for by an ionospheric current of broad latitudinal dimensions similar to the DPC current previously suggested by Feldstein (1969) to account for quiet time surface field variations at high latitudes. The positive ΔB region contains a contribution from the westward electrojet, but its characteristics cannot be completely accounted for by ionospheric currents, i.e., part of the positive ΔB apparently comes from a magnetospheric source.

The disturbance magnitude in the negative ΔB region increases from winter to equinox to summer and also increases with increasing Ap. This seasonal change is that expected from ionospheric currents, as the conductivity in this region is presumably mainly determined by solar radiation. Because solar radiation is unaffected by magnetic activity, the increase of disturbance magnitude with Ap in the negative ΔB region indicates that the electric fields driving the ionospheric currents must increase, on the average, with magnetic activity.

13

Our data do not, however, permit complete separation of effects due to increased electric field magnitude from any effects which may be due to conductivity enhancement due to increased particle precipitation.

It can be noted from Figure 6 that if the ΔB vs. Ap curves are projected to Ap equal zero, the disturbance in the positive ΔB region is very close to zero. This is not true in the negative ΔB region for data below 550 km. There is some question if such a projection is valid when only four levels of disturbance are sampled, but our impression from scanning individual passes through the region where the peak negative ΔB occurs is that some negative ΔB is usually present, even on otherwise very quiet days, during the summer. Completely quiet passes are much more common during winter. This would confirm the results of Fukushima (1962) who, using individual station K-indices, showed that magnetic disturbance at the earth's surface is present in the sunlit polar cap region even during periods of magnetic quiet at lower latitudes.

ACKNOWLEDGMENTS

REFERENCES

Armstrong, J. C., and A. J. Zmuda, Field aligned current at 1100 km in the auroral region measured by satellite, J. Geophys. Res., 75, 7122, 1970.

Cain, J. C., R. A. Langel, and S. J. Hendricks, First magnetic field results from the OGO-2 satellite, Space Res., VII, 1467, 1967a.

Cain, J. C., S. J. Hendricks, R. A. Langel, and W. V. Hudson, A proposed model for the International Geomagnetic Reference Field-1965, J. Geomagnet. Geoelec., 19, 335-355, 1967b.

Cain, J. C., and R. A. Langel, Geomagnetic survey by the Polar Orbiting Geophysical Observatories, World Magnetic Survey, ed., A. J. Zmuda, IAGA Bull. No. 28, Paris, 1971.

Farthing, W. H., and W. C. Folz, Rubidium vapor magnetometer for near earth orbiting spacecraft, Rev. Sci. Instr., 38, 1023-1030, 1967.

Feldstein, Y. I., Polar auroras, polar substorms, and their relationships with the dynamics of the magnetosphere, Rev. Geophys., 7, 179-218, 1969.

Fukushima, N., Gross character of geomagnetic disturbance during the International Geophysical Year and the Second Polar Year, Rep. Ionos. Space Res. Japan, 16, 37-56, 1962.

Langel, R. A., Processing of the total field magnetometer data from the OGO-2 satellite, NASA/GSFC Report X-612-67-272, Goddard Space Flight Center, Greenbelt, Md., June 1967.

Langel, R. A., A study of high latitude magnetic disturbance, Thesis, Univ. of Maryland, 1973. Also published as Technical Note BN-767, Institute for Fluid Dynamics and Applied Mathematics, Univ. of Maryland, 1973.

Zmuda, A. J., F. T. Heuring, and J. H. Martin, Transverse magnetic disturbances at 1100 kilometers in the auroral region, J. Geophys. Res., 71, 5033-5045, 1966.

Zmuda, A. J., F. T. Heuring, and J. H. Martin, Dayside magnetic disturbances at 1100 kilometers in the auroral oval, J. Geophys. Res., 72, 1115-1117, 1967.

Table 1

POGO(8/71) Coefficients, Epoch 1960.0

N	M	$g_n^m \, (\gamma)$	$h_n^m \, (\gamma)$	$\dot{g}_n^m \, (\gamma/\mathrm{yr})$	$\dot{h}_n^m \, (\gamma/\mathrm{yr})$
1	0	–30460.9	0.0	24.5	0.0
1	1	–2175.0	5808.9	10.4	–6.3
2	0	–1543.7	0.0	–23.4	0.0
2	1	2997.4	–1988.2	0.3	–5.0
2	2	1567.6	212.4	3.9	–20.3
3	0	1308.5	0.0	–3.2	0.0
3	1	–1984.4	–440.8	–11.1	7.1
3	2	1311.0	277.6	–1.6	1.5
3	3	868.4	–144.9	–3.3	–1.7
4	0	959.8	0.0	–0.9	0.0
4	1	812.5	130.8	–1.2	3.8
4	2	506.0	–280.6	–4.4	2.1
4	3	–382.6	3.2	–1.2	0.9
4	4	274.0	–267.8	1.3	–2.9
5	0	–223.3	0.0	1.2	0.0
5	1	358.8	12.4	0.1	1.2
5	2	240.8	115.6	1.0	2.5
5	3	–23.6	–112.8	–1.4	–3.6
5	4	–151.3	–120.5	–0.9	1.9
5	5	–48.8	93.3	1.6	–1.5
6	0	46.8	0.0	–0.0	0.0
6	1	58.3	–6.7	0.4	–0.6
6	2	–1.5	108.5	1.8	–0.9
6	3	–242.0	68.1	2.7	1.2
6	4	–1.8	–21.0	–1.1	–1.3
6	5	–3.2	–25.0	0.7	2.0
6	6	–71.9	–22.5	–2.7	0.8

Table 1 (continued)

N	M	$g_n{}^m(\gamma)$	$h_n{}^m(\gamma)$	$\dot{g}_n{}^m(\gamma/\text{yr})$	$\dot{h}_n{}^m(\gamma/\text{yr})$
7	0	72.5	0.0	-0.4	0.0
7	1	-51.1	-54.7	-0.3	-1.6
7	2	4.6	-25.9	-0.0	-0.2
7	3	12.7	-7.4	0.2	0.4
7	4	-35.2	13.3	1.1	0.3
7	5	-7.4	21.2	-0.0	0.1
7	6	14.7	-18.8	0.2	-0.1
7	7	1.7	-32.0	-0.9	1.3
8	0	7.7	0.0	0.4	0.0
8	1	4.5	10.7	0.1	-0.2
8	2	-5.9	-13.5	0.4	-0.0
8	3	-11.9	6.0	0.1	-0.5
8	4	-1.8	-18.2	0.1	-0.1
8	5	7.0	12.4	-0.2	-0.7
8	6	-18.5	23.4	1.4	0.0
8	7	18.2	0.2	-0.2	-0.6
8	8	20.9	-23.1	-1.5	0.3
9	0	12.2	0.0	-0.1	0.0
9	1	6.4	-20.0	0.2	-0.1
9	2	3.0	15.5	-0.4	0.1
9	3	-12.1	1.3	0.1	0.3
9	4	15.1	-5.2	-0.4	-0.1
9	5	1.5	0.5	-0.1	-0.5
9	6	0.3	9.4	-0.3	-0.1
9	7	1.0	15.2	0.3	-0.4
9	8	6.8	-0.4	-0.1	-0.3
9	9	2.8	-7.8	-0.5	1.2

Table 1 (continued)

N	M	$g_n{}^m (\gamma)$	$h_n{}^m (\gamma)$	$\dot{g}_n{}^m (\gamma/yr)$	$\dot{h}_n{}^m (\gamma/yr)$
10	0	-2.5	0.0	0.0	0.0
10	1	-2.2	3.0	-0.0	-0.1
10	2	3.3	1.9	-0.1	-0.0
10	3	-2.6	1.1	-0.2	0.3
10	4	-2.0	6.1	-0.0	-0.0
10	5	9.0	-5.6	-0.2	0.1
10	6	10.0	0.6	-0.5	-0.1
10	7	-1.5	-5.0	0.0	0.3
10	8	-1.9	5.0	0.1	-0.0
10	9	4.0	0.6	-0.1	-0.0
10	10	-1.1	-3.5	0.1	-0.3

Table 2

Characteristics of Average Plots

θ_{sun}	Pole	Alt < 550			550 < Alt < 700			700 < Alt < 900			Alt > 900		
		$\overline{Alt}$	$\overline{N}$	$\overline{Ap}$	$\overline{Alt}$	$\overline{N}$	$\overline{Ap}$	$\overline{Alt}$	$\overline{N}$	$\overline{Ap}$	$\overline{Alt}$	$\overline{N}$	$\overline{Ap}$
Kp = 0 to 0$^+$													
$\lvert\theta_s\rvert <$ 10°	N	452	9.0	1.6	621	4.6	1.5	802	6.6	1.5	1119	5.5	1.4
$\lvert\theta_s\rvert <$ 10°	S	471	6.0	1.5	624	4.4	1.6	811	7.9	1.6	1212	10.4	1.3
$\theta_s <$ -10°	N	457	10.0	1.1	622	5.7	1.3	795	7.9	1.3	1199	8.3	1.2
$\theta_s <$ -10°	S	476	7.3	1.4	624	6.6	1.3	801	9.1	1.3	1245	12.6	1.1
$\theta_s >$ 10°	N	455	6.1	1.8	620	4.2	1.9	795	5.0	1.8	1132	4.3	1.7
$\theta_s >$ 10°	S	464	5.3	1.7	628	3.4	1.7	805	5.0	1.8	1081	6.4	1.8
Kp = 1$^-$ to 1$^+$													
$\lvert\theta_s\rvert <$ 10°	N	451	19.8	3.9	624	8.2	3.9	807	15.0	4.0	1156	8.9	3.8
$\lvert\theta_s\rvert <$ 10°	S	468	14.3	4.0	623	8.3	3.9	813	18.4	3.9	1186	16.8	4.0
$\theta_s <$ -10°	N	459	19.5	3.9	624	11.3	4.0	801	20.8	4.0	1209	11.7	4.0
$\theta_s <$ -10°	S	469	20.2	4.0	623	12.7	4.0	806	20.2	4.0	1162	15.1	3.9
$\theta_s >$ 10°	N	452	22.1	4.1	620	10.4	4.1	799	16.5	4.1	1135	8.1	3.9
$\theta_s >$ 10°	S	466	14.9	4.1	626	8.5	4.1	808	15.0	4.1	1079	22.7	4.0

$\overline{ALT}$ is average altitude in kilometers.

$\overline{N}$ is average number of points per subdivision in average plot.

$\overline{Ap}$ is average Ap.

Table 2 (continued)

θ_{sun}	Pole	Alt < 550			550 < Alt < 700			700 < Alt < 900			Alt > 900		
		$\overline{Alt}$	$\overline{N}$	$\overline{Ap}$	$\overline{Alt}$	$\overline{N}$	$\overline{Ap}$	$\overline{Alt}$	$\overline{N}$	$\overline{Ap}$	$\overline{Alt}$	$\overline{N}$	$\overline{Ap}$
						Kp = 2$^-$ to 3$^+$							
$|\theta_s| < 10°$	N	455	32.1	10.4	622	15.1	10.7	809	25.9	10.8	1149	12.3	10.5
$|\theta_s| < 10°$	S	467	25.7	10.9	624	15.8	10.7	811	30.9	10.6	1139	19.8	10.4
$\theta_s < -10°$	N	459	31.2	10.7	623	19.4	10.7	807	35.4	10.5	1227	17.4	10.6
$\theta_s < -10°$	S	466	36.0	10.6	624	21.7	10.7	807	32.4	10.9	1154	19.6	10.4
$\theta_s > 10°$	N	453	37.8	9.9	619	15.3	10.7	800	26.1	11.0	1107	9.8	10.2
$\theta_s > 10°$	S	465	24.5	11.0	626	13.5	10.8	811	30.7	10.2	1055	27.9	9.6
						Kp $\geqslant$ 4$^-$							
$|\theta_s| < 10°$	N	465	11.0	35.4	622	8.6	47.7	809	12.8	40.8	1189	6.2	35.7
$|\theta_s| < 10°$	S	465	11.7	40.2	626	7.8	46.3	803	12.1	36.3	1148	7.7	39.5
$\theta_s < -10°$	N	459	10.1	34.6	627	6.8	41.7	799	11.7	35.2	1197	5.2	30.4
$\theta_s < -10°$	S	473	10.6	34.7	623	7.4	40.0	813	12.5	34.3	1167	5.9	35.3
$\theta_s > 10°$	N	463	8.8	42.5	617	5.4	37.0	801	7.7	36.8	1177	3.1	37.9
$\theta_s > 10°$	S	462	7.2	37.2	630	4.7	38.6	800	8.5	46.0	1071	5.9	35.1

$\overline{ALT}$ is average altitude in kilometers.

$\overline{N}$ is average number of points per subdivision in average plot.

$\overline{Ap}$ is average Ap.

Table 3

Comparison of Contours of Maximum Disturbance

Kp Range	$0-0^+$	$1^- - 1^+$	$2^- - 3^+$	$\geqslant 4^-$	$0-0^+$	$1^- - 1^+$	$2^- - 3^+$	$\geqslant 4^-$	$0-0^+$	$1^- - 1^+$	$2^- - 3^+$	$\geqslant 4^-$
Positive ΔB												
Altitude Range	Northern Summer				Northern Winter				Northern Equinox			
<550	15	20	48	120	10	21	51	109	11	18	55	120
550 – 700	10	14	52	120	18	18	48	150*	5	18	43	110
700 – 900	8	11	34	84	17	22	45	92	10	20	43	90
>900	8	12	35	50*	7	22	31	75*	—	—	—	—
Altitude Range	Southern Summer				Southern Winter				Southern Equinox			
<550	5	23	55	140	22	25	59	84	10	25	50	109
550 – 700	6	12	37	94	20	25	37	98	10	27	44	98
700 – 900	8	15	39	88	20	20	40	130	15	18	45	110
>900	2	10	25	51*	15	17	30	65*	10	15	35	79

Altitudes are in kilometers, contour levels (ΔB) in gamma.
Asterisks indicate regions where few points entered into the averages.
Five or more average points are within each contour.

Table 3 (continued)

Kp Range	$0 - 0^+$	$1^- - 1^+$	$2^- - 3^+$	$\geqslant 4^-$	$0 - 0^+$	$1^- - 1^+$	$2^- - 3^+$	$\geqslant 4^-$	$0 - 0^+$	$1^- - 1^+$	$2^- - 3^+$	$\geqslant 4^-$
Negative ΔB												
Altitude Range	Northern Summer				Northern Winter				Northern Equinox			
<550	-33	-47	-81	-105	-16	-15	-23	-42	-7	-20	-42	-71
550 - 700	-17	-35	-53	-90	-6	-7	-14	-28	-10	-15	-31	-53
700 - 900	-10	-27	-40	-66	0	0	-7	-9	-5	-9	-18	-35
>900	-2	-12	-30	-55*	0	—	0	-4*	—	-5	-13	-24
Altitude Range	Southern Summer				Southern Winter				Southern Equinox			
<550	-25	-36	-87	-115	-10	-17	-24	-50	-10	-16	-57	-73
550 - 700	-20	-37	-57	-130	-3	-11	-14	-45	-10	-12	-33	-62
700 - 900	-10	-20	-38	-65	0	-1	-9	-20	—	-5	-17	-36
>900	-10(?)	-14	-21	-39*	0	—	0	-2	—	-2	-10	-25

Altitudes are in kilometers, contour levels (ΔB) in gamma.
Asterisks indicate regions where few points entered into the averages.
Five or more average points are within each contour.

Table 4

Approximate Standard Error of Averages (gamma)

Kp Range	$0 - 0^+$	$1^- - 1^+$	$2^- - 3^+$	$\geqslant 4^-$	$0 - 0^+$	$1^- - 1^+$	$2^- - 3^+$	$\geqslant 4^-$	$0 - 0^+$	$1^- - 1^+$	$2^- - 3^+$	$\geqslant 4^-$
Positive ΔB Region												
Altitude Range	Northern Summer				Northern Winter				Northern Equinox			
<550	6.1	4.3	7.8	40.0	3.2	4.8	9.1	34.3	3.7	4.0	9.7	36.2
550 - 700	4.9	4.3	13.3	51.6	7.5	5.4	10.9	57.5	2.3	6.3	11.1	37.5
700 - 900	3.6	2.7	6.7	30.3	6.0	4.8	7.6	26.9	3.9	5.2	8.4	25.2
>900	3.9	4.2	11.2	28.4	2.4	6.4	7.4	32.9	—	—	—	—
Altitude Range	Southern Summer				Southern Winter				Southern Equinox			
<550	1.9	5.1	9.2	43.0	9.6	6.5	11.9	31.3	4.1	6.6	9.9	31.9
550 - 700	2.3	3.4	7.9	34.6	10.8	8.6	10.1	45.2	4.8	9.4	11.1	35.1
700 - 900	2.7	3.3	6.9	24.9	8.9	5.2	7.2	44.6	5.3	4.2	8.1	31.6
>900	0.6	2.6	5.6	21.0	5.9	3.6	5.7	26.8	3.1	3.7	7.9	28.5

Altitudes are in kilometers.

24

Table 4 (continued)

| Kp Range	0 – 0⁺	1⁻ – 1⁺	2⁻ – 3⁺	≥4⁻	0 – 0⁺	1⁻ – 1⁺	2⁻ – 3⁺	≥4⁻	0 – 0⁺	1⁻ – 1⁺	2⁻ – 3⁺	≥4⁻
Negative ΔB Region												
Altitude Range	Northern Summer				Northern Winter				Northern Equinox			
<550	13.4	10.0	13.2	35.4	5.1	3.4	4.1	13.2	2.3	4.5	7.4	21.4
550 – 700	8.3	10.9	13.5	38.7	2.5	2.1	3.2	10.7	4.7	5.2	8.0	18.1
700 – 900	4.5	6.6	7.8	23.8	—	—	1.2	2.6	1.9	2.3	3.5	9.8
>900	1.0	4.2	9.6	31.2	—	—	—	1.8	—	1.7	3.7	9.6
Altitude Range	Southern Summer				Southern Winter				Southern Equinox			
<550	9.3	8.0	14.5	35.3	4.3	4.4	4.8	18.6	4.1	4.2	11.2	21.3
550 – 700	7.8	10.4	12.2	47.8	1.6	3.8	3.8	20.8	4.8	4.2	8.3	22.2
700 – 900	3.3	4.4	6.7	18.5	—	0.3	1.6	6.9	—	1.2	3.1	10.3
>900	2.8	3.6	4.7	16.1	—	—	—	0.8	—	0.5	2.2	9.0

Altitudes are in kilometers.
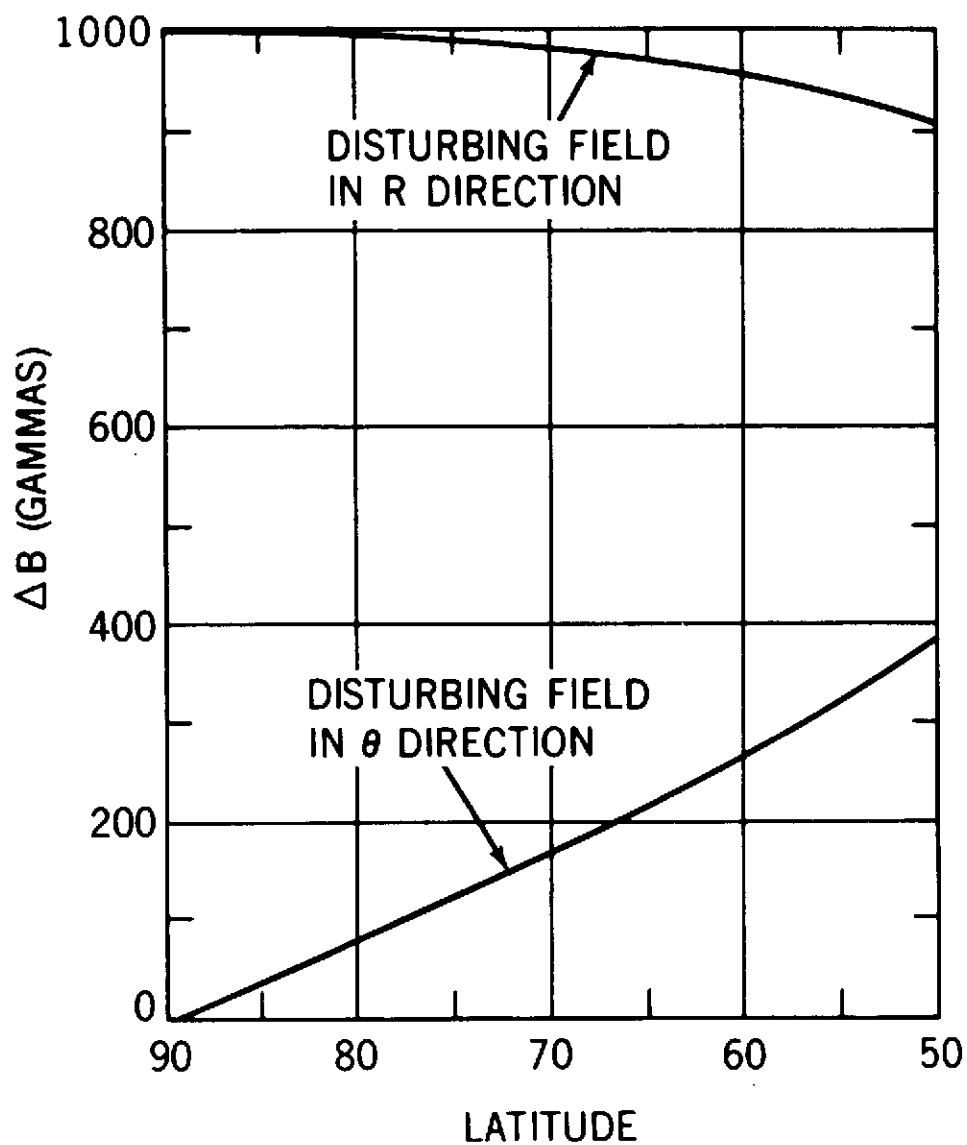
Figure 1. ΔB, resulting from a disturbing field of 1000γ, as a function of latitude. The earth's field is represented by a centered dipole. These results are unchanged with altitude from 1.0 Re to 1.3 Re.
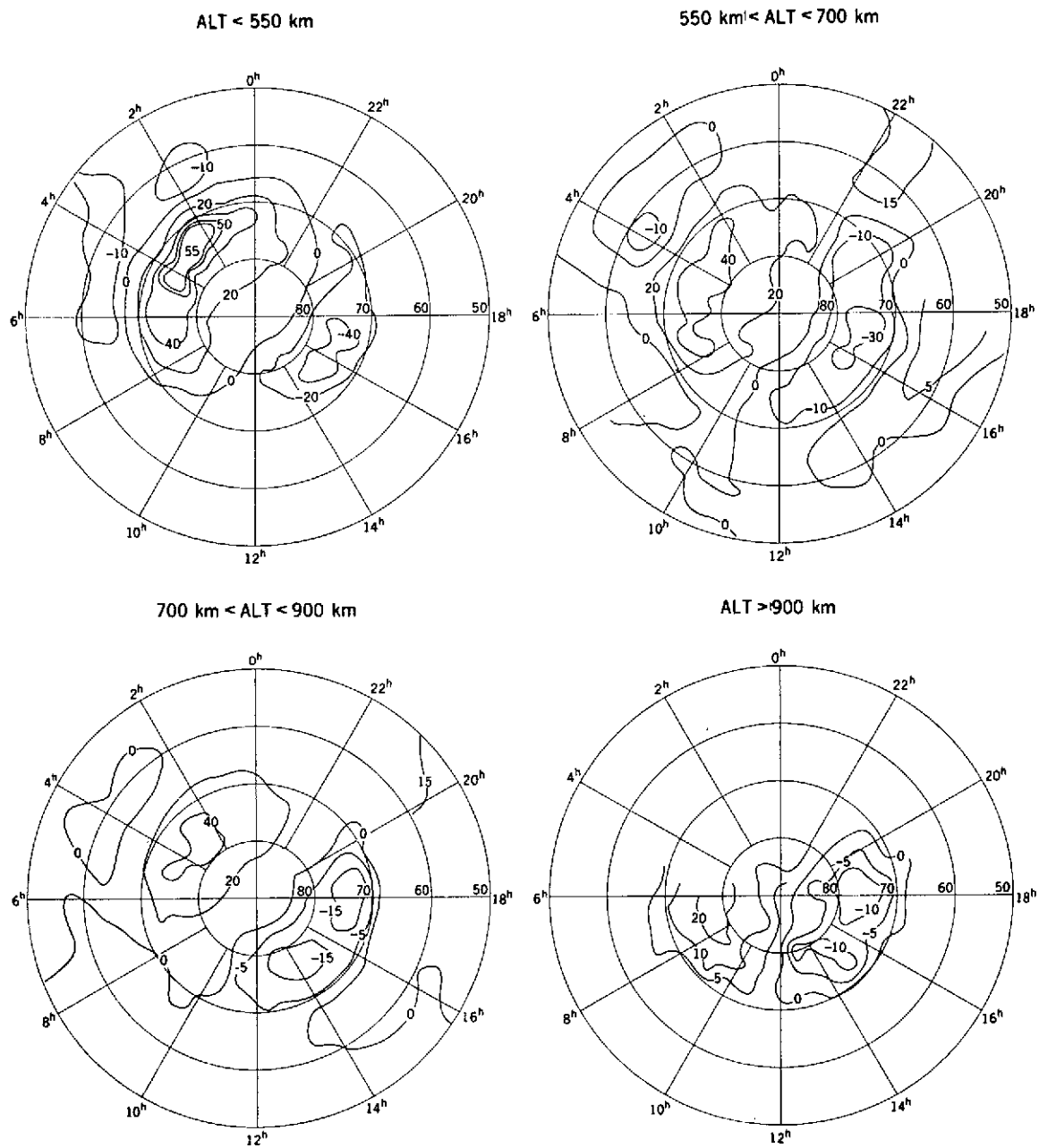
ALT < 550 km

550 km < ALT < 700 km

700 km < ALT < 900 km

ALT > 900 km

Figure 2. Average △B from OGO 2, 4, and 6 for Kp = 2⁻ to 3⁺, northern hemisphere, and Geomagnetic Equinox. Coordinates are invariant latitude and magnetic local time.
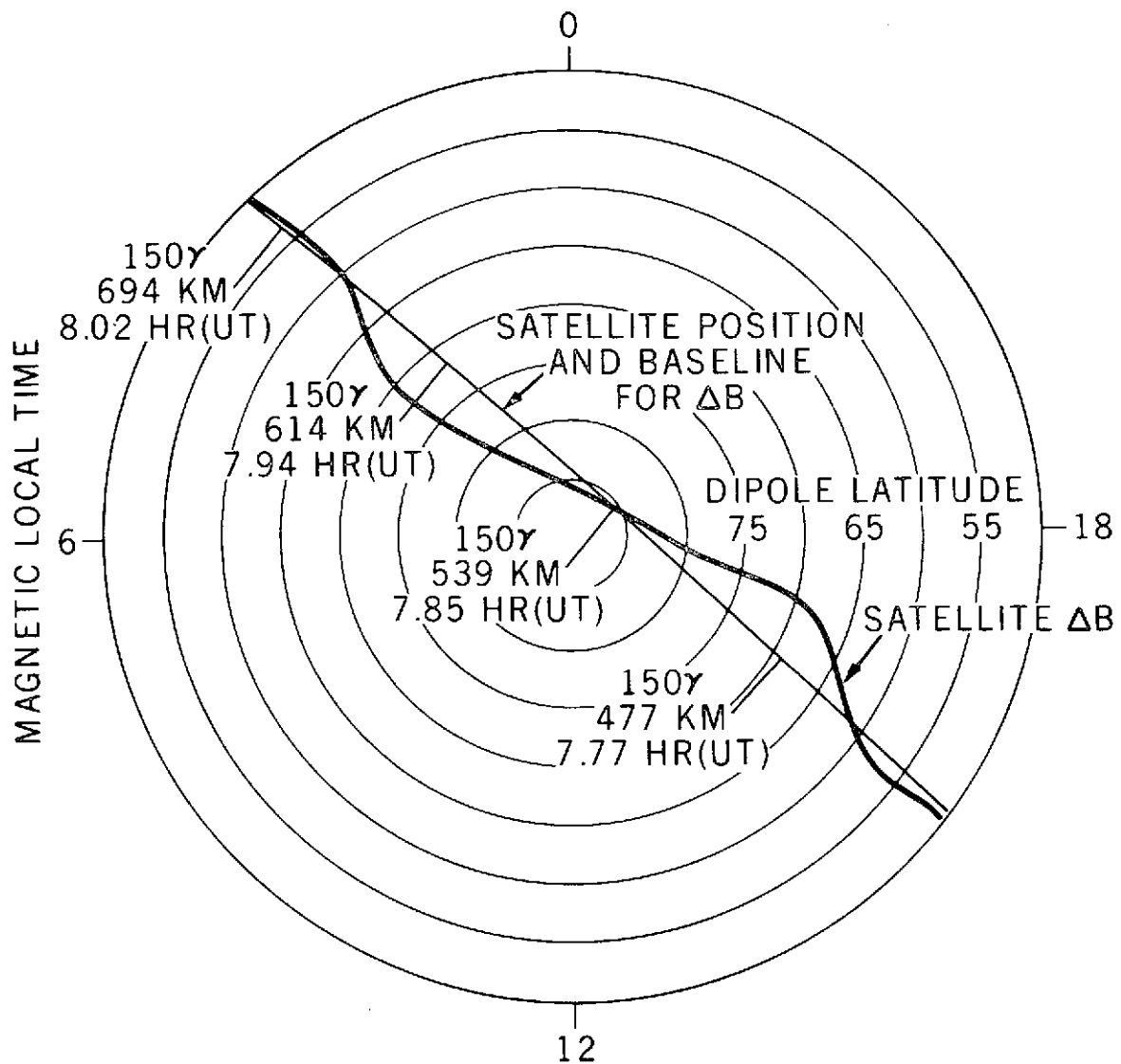
Figure 3. Typical example of a satellite pass through both the positive and the negative ΔB regions. Data are from OGO 4 on 9/1/67, northern hemisphere. The length of the scale lines gives the scale for 150γ of ΔB; the altitude (km.) and universal time (hour and fraction thereof) are indicated at each scale line.
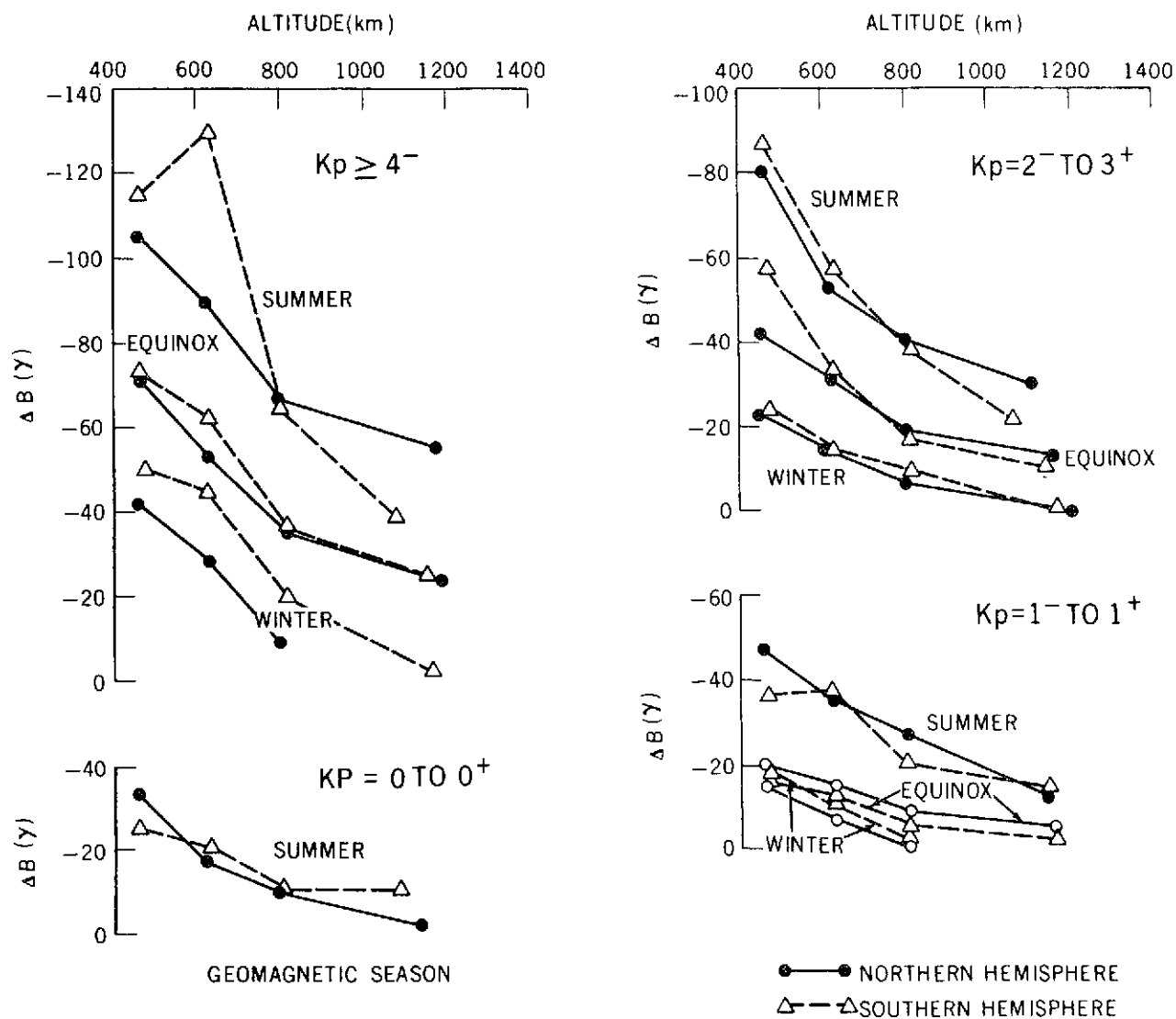
Figure 4. Variation with altitude of ΔB from the contour of maximum disturbance in the negative ΔB region.

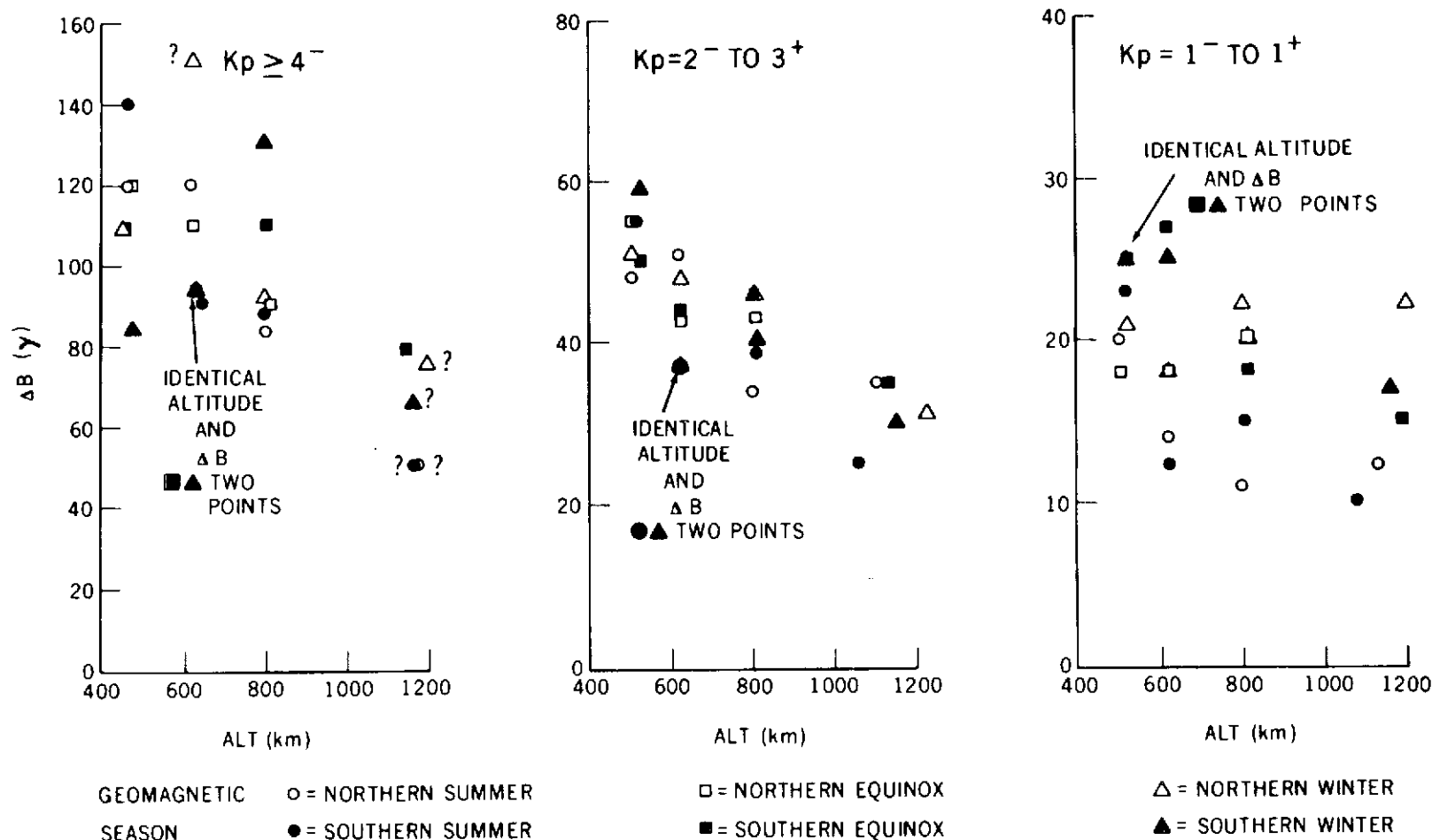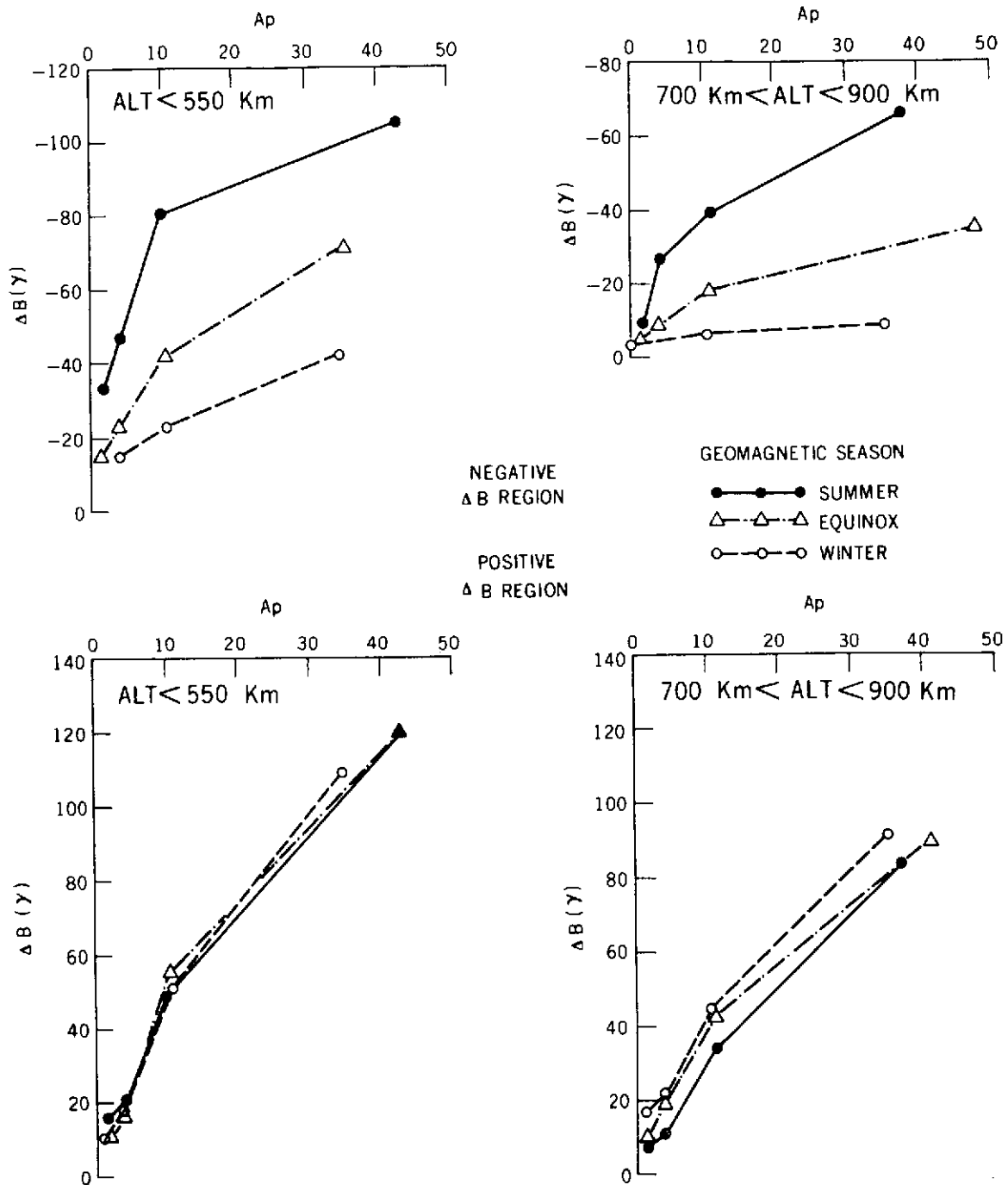Figure 5. Variation with altitude of ΔB from the contour of maximum disturbance in the positive ΔB region.

Figure 6.   Variation with Ap of ΔB from the contour of maximum disturbance.